

Synthesis and characterization of silica doped alumina catalyst support with superior thermal stability and unique pore properties

Maryam Khosravi Mardkhe¹ · Baiyu Huang¹ · Calvin H. Bartholomew² · Todd M. Alam³ · Brian F. Woodfield¹

Published online: 21 November 2015
© Springer Science+Business Media New York 2015

Abstract A facile, solvent-deficient, one-pot synthesis of a thermally stable silica-doped alumina, having high surface area, large pore volume and uniquely large pores, has been developed. Silica-doped alumina (SDA) was synthesized by adding 5 wt% silica from tetraethyl orthosilicate (TEOS) to aluminum isopropoxide (AIP), a 1:5 mol ratio AIP to water, and a 1:2 mol ratio TEOS to water in the absence of a template. The structure of silica-doped alumina was studied by in situ high-temperature powder XRD, nitrogen adsorption, thermogravimetric analysis, solid-state NMR, and TEM. The addition of silica significantly increases the stability of γ -Al₂O₃ phase to 1200 °C while maintaining a high surface area, a large pore volume and a large pore diameter. After calcination at 1100 °C for 2 h, a surface area of 160 m²/g, pore volume of 0.99 cm³/g, and a bimodal pore size distribution of 23 and 52 nm are observed. Compared to a commercial silica-doped alumina, after calcination for 24 h at 1100 °C, the surface area, pore volume, and pore diameter SDA are higher by 46, 155, and 94 %, respectively. Results reveal that Si stabilizes the porous structure of γ -Al₂O₃ up to 1200 °C, while unstabilized alumina is stable to only 900 °C. From our data, we infer that Si enters tetrahedral vacancies in the defect spinel

structure of alumina without moving Al from tetrahedral positions and forms a silica–alumina interface.

Keywords Silica-doped alumina · Thermally stable · Large pore size · High surface area

1 Introduction

Gamma alumina (γ -Al₂O₃) is one of the most widely used commercial catalyst supports because of its moderately high surface area, meso- and macro-porosity and relatively high thermal and hydrothermal stabilities. It is an effective catalyst support for both base and noble metals in many different applications: e.g., Pt/Pd catalytic converters [1], Ni catalyst in hydrogenation [2], Co(Ni)–Mo(W) sulfide catalysts for hydrotreating of petroleum feed stocks [3], and Co catalyst for Fischer–Tropsch synthesis (FTS) [4, 5]. Since each of these applications typically requires a unique range of surface area, pore volume and pore diameter, commercial aluminas are supplied with a wide range of surface areas and porosities [6–8]. Therefore, the ability to optimize γ -Al₂O₃ porosity is vital in the manufacture of these materials [4, 9–11].

While γ -Al₂O₃ is stable during long term use at 500–600 °C, at higher reaction temperatures (650–1100 °C) and especially in the presence of water vapor, the porous structure collapses due to sintering and structural transformations to other forms of alumina (α -Al₂O₃), resulting in lower porosity of the supports, and in some cases, deactivation of the catalyst. Thus, in a number of catalytic reactions taking place at elevated temperatures and high steam concentrations, e.g. auto emissions control and steam reforming [12–17], the thermal and hydrothermal stability of γ -Al₂O₃ is inadequate. Nevertheless, γ -

✉ Brian F. Woodfield
Brian_woodfield@byu.edu

¹ Department of Chemistry and Biochemistry, Brigham Young University, Provo, UT 84602, USA

² Department of Chemical Engineering, Brigham Young University, Provo, UT 84602, USA

³ Department of Electronic, Optical and Nanostructured Materials, Sandia National Laboratories, Albuquerque, NM 87185, USA

Al₂O₃ can be stabilized against sintering and phase transformations through the incorporation of suitable dopants (i.e. alkaline earth oxides, transition, and rare-earth elements, as well as SiO₂). Previous studies have demonstrated that thermal and hydrothermal stabilities of alumina are substantially improved by the addition of 1–20 wt% silica [15–21], titania [22, 23], zirconia [19, 24, 25], and rare earth elements such as lanthanum [1, 13, 26], magnesium [25, 27], and ceria [12, 28, 29].

Of particular pertinence to the present work is the use of silica at 1–10 wt% as a stabilizer for γ -Al₂O₃. A number of previous papers and patents address the preparation of stable silica-doped alumina. In an early patent, a multi-step co-gel preparation method was reported to produce silica–alumina with high porosity: the alumina sample contained 7 % silica, with a surface area of 150 m²/g, and a pore volume of 0.9 cm³/g at 1100 °C (no pore diameter was reported) [30]. This method involves the reaction of an alkali metal aluminate and silicate, followed by filtration, washing, and drying. Preparation of silica-modified-alumina with 2–10 % silica using a different co-gel method has also been reported: after calcination at 648 °C, the 5 % silica sample was reported to have a moderately high surface area of 318 m²/g and relatively low pore volume of 0.46 cm³/g [31]. This method uses acid in the sol preparation and base in the gelation step. Wan et al. [32] reported a stabilized 5.5 % silica–alumina support produced by impregnating alumina with polyorgano silane; after calcination at 1100 and 1200 °C, the surface area was 158.2 and 93 m²/g, respectively; however, neither pore volume nor pore diameter data were reported. Other complex methods involving solvents and pH adjustment techniques have also been used to make stable silica-doped alumina [12, 16, 18, 33]. However, these particular supports do not maintain high surface areas and pore volumes at higher temperatures. For example, Shutilov et al. [16] used an impregnation method to make a stable silica-doped alumina but reported low values for both surface area (68 m²/g) and pore volume (0.34 cm³/g) and a moderately large pore diameter (15 nm) at 1100 °C. Zhao et al. [34] studied the effect of dopants, including silica, on the alumina supports for Rh catalysts. However, the surface area of the silica doped alumina after calcination at 1200 °C, i.e. 55 m²/g, was still relatively low. Silica-doped aluminas having high surface area and pore volume at high temperatures have also been synthesized using aerogel and cryogel methods, but they are costly and time consuming [15, 17, 20]. For example, Miller et al. [15] produced a stable silica-doped alumina containing 10 % silica by the multi-step aerogel method and using supercritical drying to remove the solvent. At 1200 °C, it has a surface area of 150 m²/g and pore volume of 0.65 cm³/g, which are unusually high for this temperature; no pore diameter data

were available. Horiuchi et al. [17] used supercritical drying to synthesize silica-doped alumina with a surface area of 110 m²/g, pore volume of 0.9 cm³/g and pore diameter of 18.6 nm at 1200 °C. Later, Horiuchi et al. [35] reported silica doped alumina with even higher surface area (150 m²/g) after calcination at 1200 °C. However, their method involved a multi-step preparation, such as peptizing, refluxing, gelation, solvent exchanging, and supercritical drying, which was relatively complex and time consuming.

From this previous work, it is evident that the addition of silica to alumina produces alumina support materials with substantially higher porosity at high temperatures (relative to pure alumina). Such materials having thermal and hydrothermal stabilities facilitate higher catalyst loadings and increase catalyst lifetime, activity, and productivity at high operating temperatures [5]. However, most of the previous preparation methods involve complex, multi-step procedures and hence higher manufacturing costs. Therefore, it would be desirable to devise simple, low-cost methods that produce such materials.

In the present work, we report a simple, one-pot, solvent-deficient preparation method for silica-doped γ -Al₂O₃ supports with high surface area, large pore volume, uniquely large pores having a bimodal distribution, and high thermal stability. The results indicate that in 5 % SDA, Si ions are incorporated into vacant tetrahedral sites of the alumina spinel and retard the phase transformation from γ to α , and therefore stabilize the alumina structure at elevated temperatures.

2 Experimental

2.1 Material

Aluminum isopropoxide (C₉H₂₁O₃Al) (granular, 98+ %) and tetraethyl orthosilicate (SiC₈H₂₀O₄) (liquid, 99.9 %) (TEOS) were purchased from Alfa-Aeser. Commercial 5 % silica-doped alumina (Siral-5) was purchased from Sasol for comparison.

2.2 Synthesis method

Silica-doped aluminas (100 g batches) (SDAs) were prepared via a patented method [36] that involves mixing aluminum isopropoxide (AIP) and water at a 5:1 mol ratio of water to AIP, then 5 wt% silica from tetraethyl orthosilicate (TEOS) and water at a 2:1 water to TEOS mole ratio. These starting materials were mixed for 30 min with a Bosch Universal Mixer at a RPM of 300. The resulted intermediate, or precursor, was then calcined at 700, 900, 1100, 1200 °C for 2 h each with 5-h ramps.

During the calcination, $\text{Al}(\text{OH})_3$ precursor decomposes leading to the formation of water and nano crystalline γ - Al_2O_3 at high temperatures and all of the byproducts were released as gases. Pure alumina [37] and samples with 15 and 27 wt% of silica were prepared for comparison.

2.3 Characterization

The alumina phase was identified by powder x-ray diffraction (XRD) using a PANalytical X'Pert Pro diffractometer with a Cu $K\alpha$ x-ray source ($\lambda = 1.5418 \text{ \AA}$) operated at 45 kV and 40 mA. Scans were performed between 10° and $90^\circ 2\theta$ with a step size of 0.0167° at a rate of 0.013°s^{-1} . The Scherrer formula was used to estimate crystallite size [38]. In situ high-temperature XRD (HTXRD) experiments were performed using this same instrument equipped with an Anton Paar HTK 1200N stage. Scans were collected using the same parameters just described as the samples were heated in purified air from 400 to 1200 °C.

Nitrogen adsorption measurements were carried out using a Micromeritics Tristar 3020 for the determination of surface properties at -196°C . Surface area was calculated using the Brunauer–Emmett–Teller (BET) model in the P/P_0 range from 0.05 to 0.20. Pore volumes were determined at a single point of P/P_0 equal to 0.990. Pore size distributions were calculated using an improved slit pore geometry (SPG) model for large pore sizes [39]. Samples were degassed at 200 °C under N_2 flow overnight before each measurement.

Microscopic images of samples were obtained with an FEI Philips Tecani F30 transmission electron microscope (TEM) at a voltage of 200 kV. TEM samples were prepared by placing a drop of silica-doped alumina (1 % dispersed in ethanol) on a carbon film with a copper mesh grid (Ted-Pella Inc.).

Thermo-gravimetric (TG) and differential-temperature (DT) analyses were performed using a NETZSCH STA 409PC instrument (NETZSCH, Germany) in the temperature range of 25–1400 °C under 20 mL/min He gas flow with a heating rate of 3 °C/min. A sample weight of 30 mg was used in a platinum pan.

Solid state MASNMR spectra were obtained on a Bruker Avance I 400 (9.6 T) instrument using a 7 mm (^{29}Si) or a 4 mm (^{27}Al) broadband MAS probe. All spectra were obtained at room temperature, and a spinning speed of 12.5 kHz for ^{27}Al or 4 kHz for ^{29}Si . The 1D ^{29}Si MAS NMR spectra used a single pulse direct polarization (DP) Block decay with a 240 s recycle delay to assure complete relaxation, while the ^1H - ^{29}Si cross polarization (CP) MAS NMR spectra was obtained using a 5 ms contact time and a 10 s recycle delay. The ^{27}Al MAS spectra were also obtained using a DP Bloch decay, and a $\pi/6$ pulse length.

The ^{27}Al chemical shift was referenced to the external secondary standard 1 M $\text{Al}(\text{H}_2\text{O})_6^+$ $\delta = 0.0$ ppm, and the ^{29}Si chemical shift was referenced to the secondary standard Q_8M_8 $\delta = +12.6$ ppm with respect to neat TMS ($\delta = 0$ ppm). Spectral simulations and deconvolutions were performed using DMFIT [40, 41]. The Czejeck distribution [42] of the ^{27}Al electrical field gradient (EFG) tensor was used in the analysis of the ^{27}Al NMR, and gives rise to the asymmetric line shapes. In some instances it was necessary to include multiple distributions for a given Al environment to reproduce the experimental line shape.

3 Results

3.1 X-ray diffraction

Figure 1 shows XRD patterns for pure alumina and three silica-doped alumina samples after calcination at 700, 900, 1100, 1200 and 1300 °C. Only characteristic broad peaks for γ - Al_2O_3 at 45.7° and 66.6° are observed at 700–900 °C for all samples; the broad lines indicate that samples consist of small crystallites of small diameter. For the pure alumina sample only α - Al_2O_3 is observed at 1200 °C (Fig. 1a). In contrast, mostly the γ - Al_2O_3 phase is observed for 5, 15, 27 % silica samples, respectively (Fig. 1b–d).

Figure 1b shows XRD patterns of 5 % silica-doped alumina (5 % SDA), calcined from 700 to 1300 °C for 2 h. Characteristic peaks of γ - Al_2O_3 , along with traces of θ - Al_2O_3 are observed for 5 % SDA after calcination at 1200 °C, suggesting that the γ phase is largely stable and the transition to the α phase has not yet occurred at this temperature. The peaks attributed to α - Al_2O_3 are not observed until 1300 °C. A comparison of these results with other published SDA materials is given below.

Figure 2 shows in situ high-temperature XRD patterns for 5 % SDA in flowing purified air. It is evident that the γ - Al_2O_3 phase in 5 % SDA is stable to 1200 °C without transforming to either θ - or α - Al_2O_3 , since no θ - or α - Al_2O_3 peaks are detected at 1200 °C. The in situ results are largely consistent with those for the ex situ furnace-calcined samples (Fig. 1b).

3.2 Nitrogen adsorption

Table 1 shows surface areas, pore volumes, and pore diameters for pure alumina and three silica-doped alumina samples, calcined at 700, 900, 1100 and 1200 °C. Pore size distributions for 5 % silica-doped alumina (SDA) calcined at different temperatures are shown in Fig. 3. The surface area and pore volume of the pure alumina sharply decreases with increasing calcination temperatures from

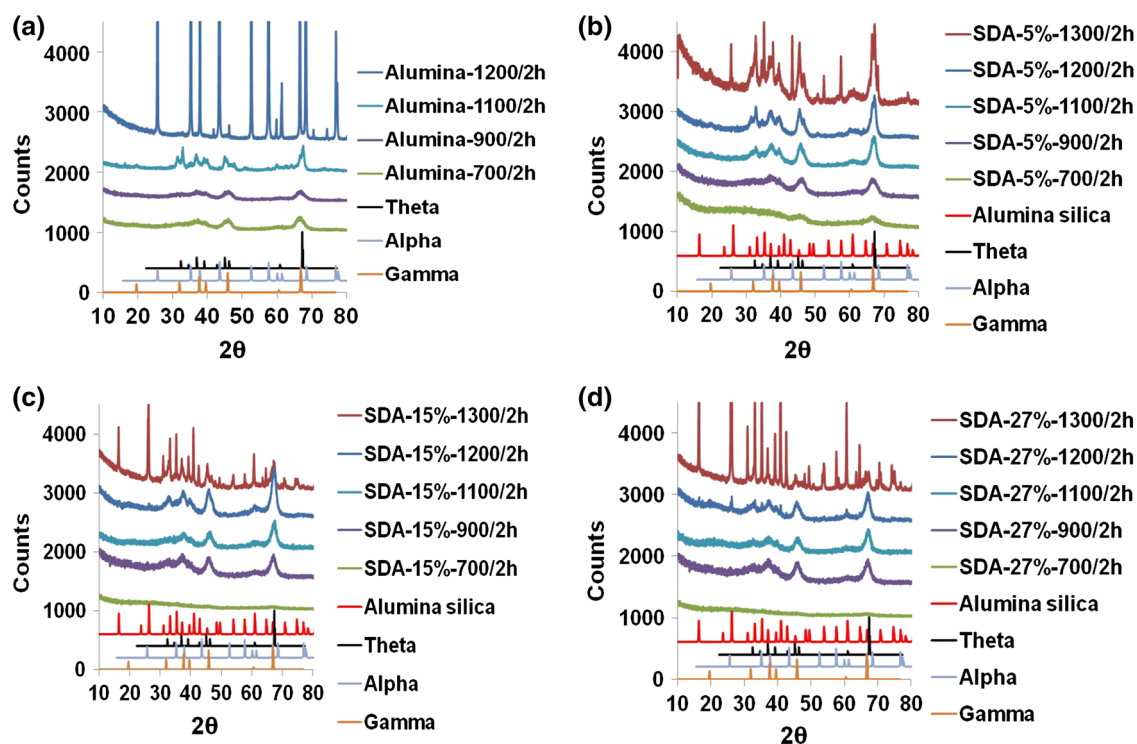


Fig. 1 XRD patterns of different aluminas calcined at different temperatures for 2 h. **a** Pure alumina, **b** 5 % SDA, **c** 15 % SDA, **d** 27 % SDA. Standards: (1) gamma alumina, (2) alpha alumina, (3) theta alumina, (4) mullite

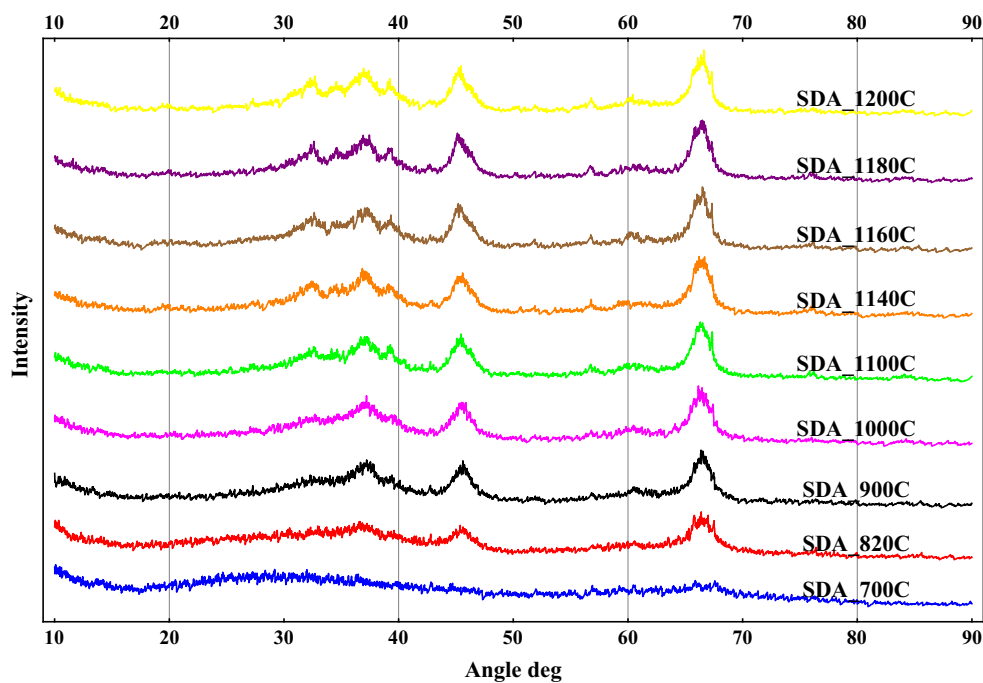


Fig. 2 In situ high-temperature XRD patterns of 5 % SDA 700–1200 °C

1100 to 1200 °C; however, the addition of silica maintained the surface area and pore volume of the aluminas. In addition, 5 % SDA shows a bimodal pore size distribution

and larger pore diameter compared to other aluminas. The 5 % SDA has a surface area of 160 m²/g, a pore volume of 0.99 cm³/g, and a bimodal pore distribution of 22.5 and

Table 1 BET results of 0–5–15–27 % SDAs calcined at different temperatures for 2 h

Silica %	Calcination T (°C/2 h)	BET surface area (m ² /g) ^a	Mesopore volume (cm ³ /g) ^a	Pore diameter (nm) ^b	SD (nm)
0 %	700	291	1.56	19.8	1.1
	900	208	1.12	25.5	1.2
	1100	119	0.77	26.7	1.6
	1200	15	0.05	0.00	–
5 %	700	378	1.83	14.7 and 35.0	1.8
	900	300	1.60	19.8 and 51.8	1.8
	1100	160	0.99	22.5 and 52.0	1.8
	1200	111	0.59	15.4 and 32.2	1.6
15 %	700	222	1.40	43.1	1.8
	900	180	1.10	39.2	1.8
	1100	146	0.96	33.6	1.6
	1200	100	0.66	31.1	1.6
27 %	700	195	1.0	51.6	1.5
	900	143	0.89	51.3	1.4
	1100	100	0.57	45.4	1.8
	1200	65	0.33	48.6	1.9

^a Determined by N₂ adsorption at 77 K

^b Determined by an improved slit pore geometry (SPG) model for large pore sizes using the desorption branch

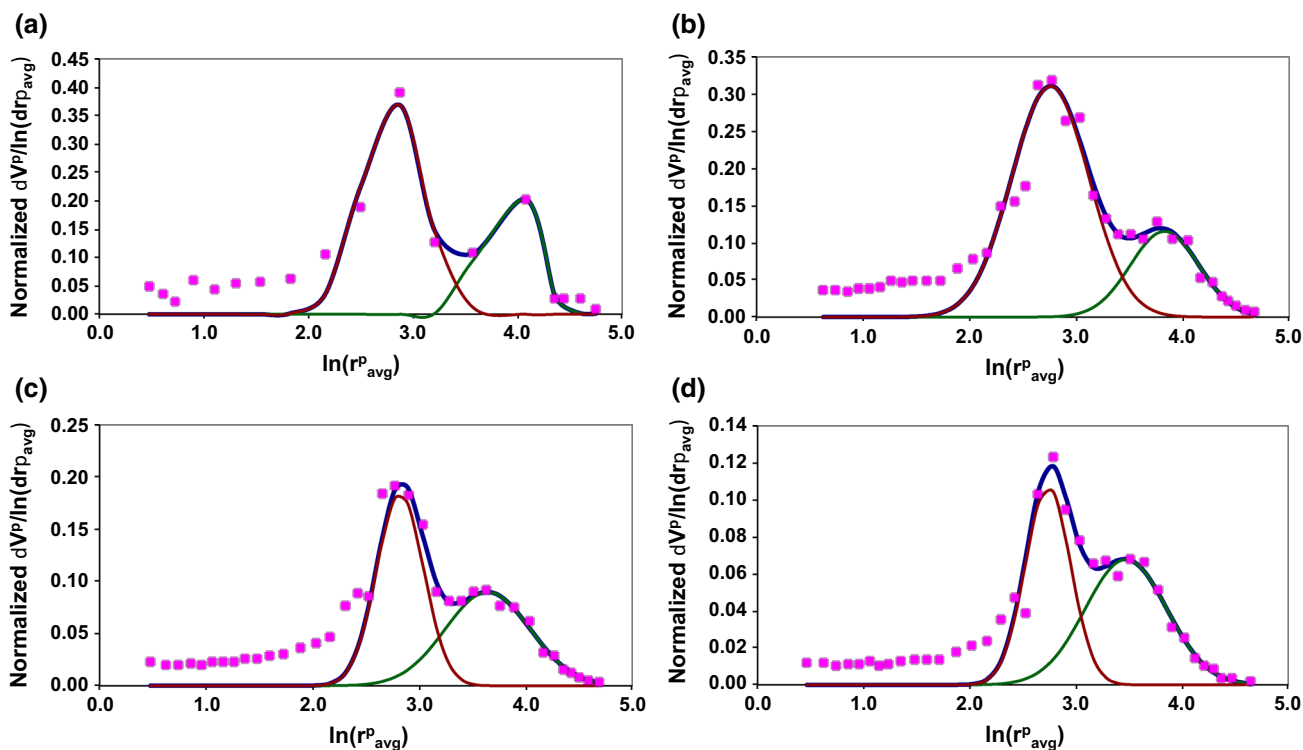


Fig. 3 Pore size distributions for 5 % SDA calcined at different temperatures for 2 h: **a** 700 °C, **b** 900 °C, **c** 1100 °C, and **d** 1200 °C

52 nm at 1100 °C. The surface area and pore volume were 111 and 0.59 cm³/g, and a bimodal pore distribution of 15.4 and 32.2 nm is observed for the same sample at 1200 °C.

3.3 TEM images

TEM images (Fig. 4a) show that primary particles of 5 % SDA are slab-like, and have a length of ca. 20 nm and a

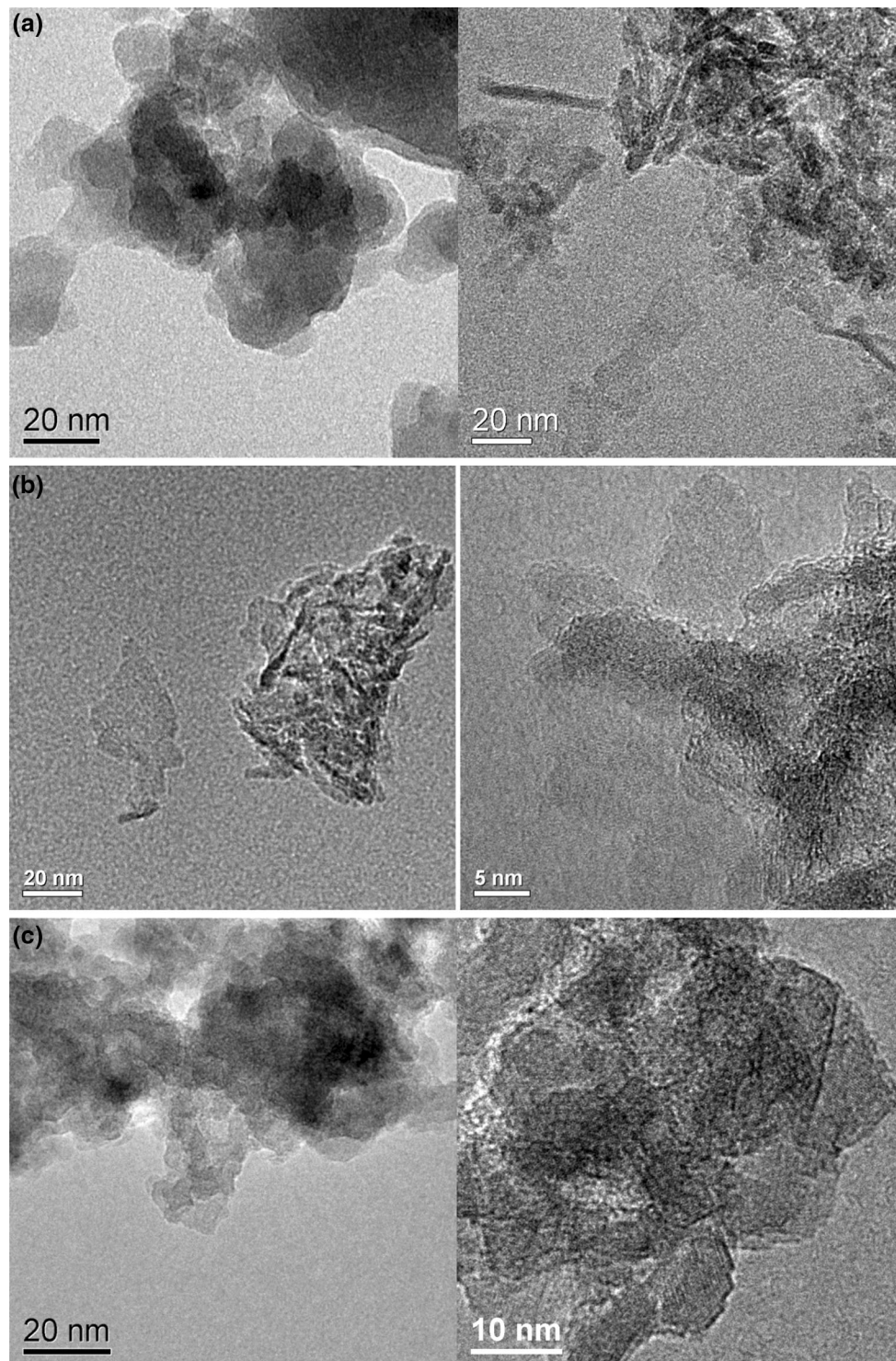


Fig. 4 TEM micrograph of aluminas calcined at different temperatures: **a** 5 % SDA calcined at 700 °C, **b** pure alumina calcined at 700 °C, **c** 5 % SDA calcined at 1100 °C

width of ca. 15 nm. Based on XRD using the Scherrer formula [38], the thickness of the slabs was calculated to be ca. 5 nm. A random three-dimensional stacking of these primary particles is also observed. The pure alumina

(Fig. 4b) has similar slab-like primary particles but less order in the stacking, which is consistent with the nitrogen adsorption results since the former possesses a larger pore volume than the latter. Consequently, at higher

temperatures (i.e. 1100 °C, Fig. 4c), the shape and size of the 5 % SDA primary particle remains relatively small; no significant grain growth is observed due to sintering from the γ - to α -Al₂O₃ phase transition, which is consistent with the XRD results.

3.4 TGA and DSC

Figure 5a shows the TG (thermogravimetric analysis) and DSC (differential scanning calorimetry) curves of the 5 % SDA sample. From the data it is clear that the weight of 5 % SDA decreases by increasing the temperature to 1400 °C. This weight loss is associated with the endothermic effect around 100 °C due to the evaporation of alcohol and physically adsorbed water. There are also three exothermic effects: first, between 800 and 1000 °C due to crystallization of the γ -Al₂O₃ phase; second between 1000 and 1300 °C due to θ -Al₂O₃ or silica–alumina phase formation and collapsing of the 3D stack structure of γ -Al₂O₃ (as shown in Fig. 4c); and third after 1300 °C due to the θ/γ phases to α -Al₂O₃ phase transition. In contrast, the γ - to α -Al₂O₃ phase transition starts at 1200 °C for pure alumina (Fig. 5b). These results confirm that the addition

of 5 wt% of silica delays the γ - to α -Al₂O₃ phase transition by 100 °C, consistent with the XRD results.

3.5 Solid state NMR measurements

Solid state ²⁷Al MAS NMR spectra for pure and 5 % silica doped alumina and corresponding deconvolutions are shown in Fig. 6. Three different major Al environments are observed: an octahedral Al(VI) environment at $\delta \sim +15$ ppm, a five-coordinated Al(V) site at $\delta \sim +40$ ppm and a tetrahedral site at +75 ppm [43–45]. Pure alumina calcined at 700 °C has 18 % of the Al in the octahedral Al(IV) environment; after adding 5 % silica, the percent of octahedral Al remains the same (18 %, 700 °C), while there is an increase in the Al(V) environment. The ²⁹Si MAS NMR and ²⁹Si-¹H CPMAS NMR spectra for 5 % SDA is shown in Fig. 7a. There is a broad overlapping resonance between (–) 81 and (–) 89 ppm. This broad resonance cross-polarizes (CP) with protons, and represents a phase in this material containing proton species (hydroxyl groups). (–) 81 ppm is assigned to Si(4Al), and (–) 89 ppm for Si(3Al) structures [45, 46]. The lack of the SiO₄ species ($\delta \sim -110$ ppm) shows that Si incorporates into Al rich coordination environments. This indicates that no separate Si domain exists in the structure. 5 % SDA (Fig. 7a) is shifted to a less negative δ in comparison to 27 % silica (Fig. 7b), most likely due to increased Al in the Si coordination sphere. For 27 % SDA (Fig. 7b) more peaks are observed due to different Si and Al coordination structures (e.g. Si(3Al), Si(2Al), Si(1Al), etc.) [4].

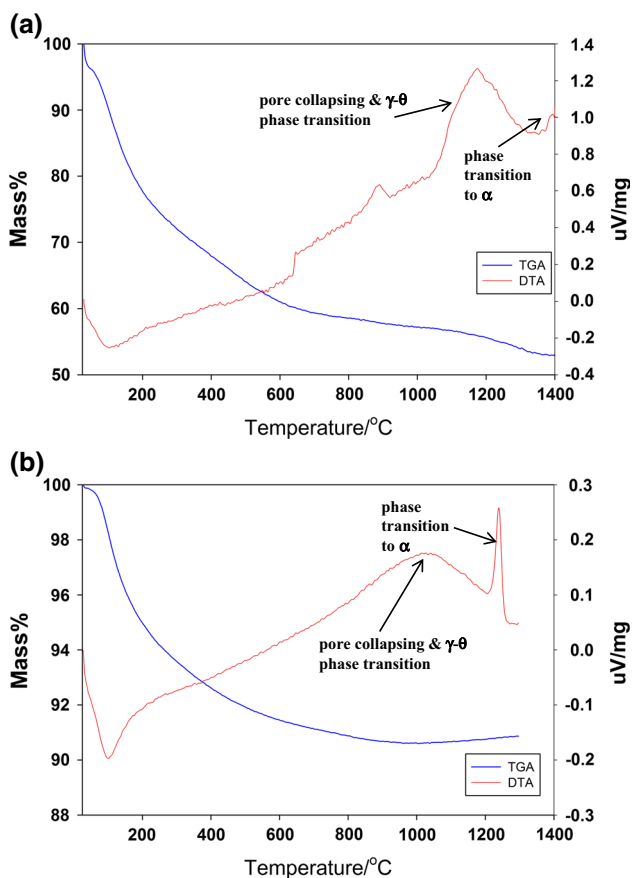


Fig. 5 Thermal analysis data for: **a** 5 % SDA, **b** pure alumina

4 Discussion

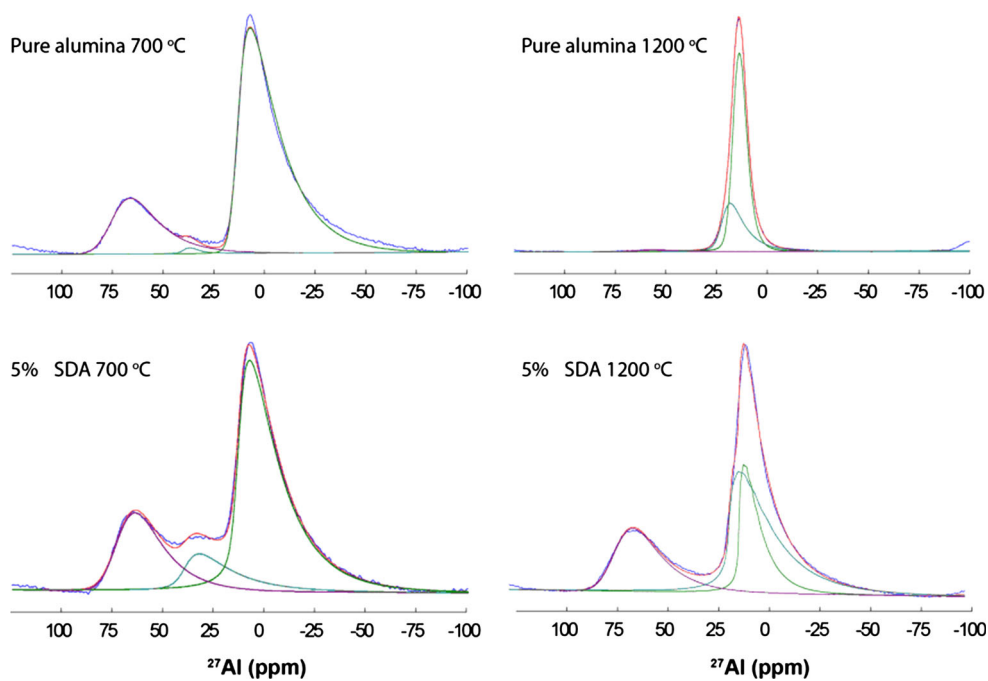
4.1 Silica–alumina structure

It is reported that alumina is a defect spinel structure, in which vacancies are distributed in both octahedral and tetrahedral sites [46]. Silica content has been theoretically calculated to be 13 %, if Si and Al fill all of the tetrahedral and octahedral sites [17, 47]. The results of this study show that ideal porosity and thermal stability of alumina are achieved by adding 5 % silica.

It was shown from ²⁷Al SSNMR data for 5 % SDA (Fig. 6) that aluminum ions in tetrahedral sites are not displaced from tetrahedral to octahedral sites by addition of silicon ions, contrary to the conclusion of Horiuchi et al. [17]; instead, Si enters the tetrahedral vacancies in the defect spinel structure of alumina and forms a Si–Al spinel phase since Al(IV) content is the same (18 %) in both pure alumina and 5 % SDA.

The results of this study confirm those reported from earlier papers [12, 15–17, 20, 21, 30–32, 48] that addition

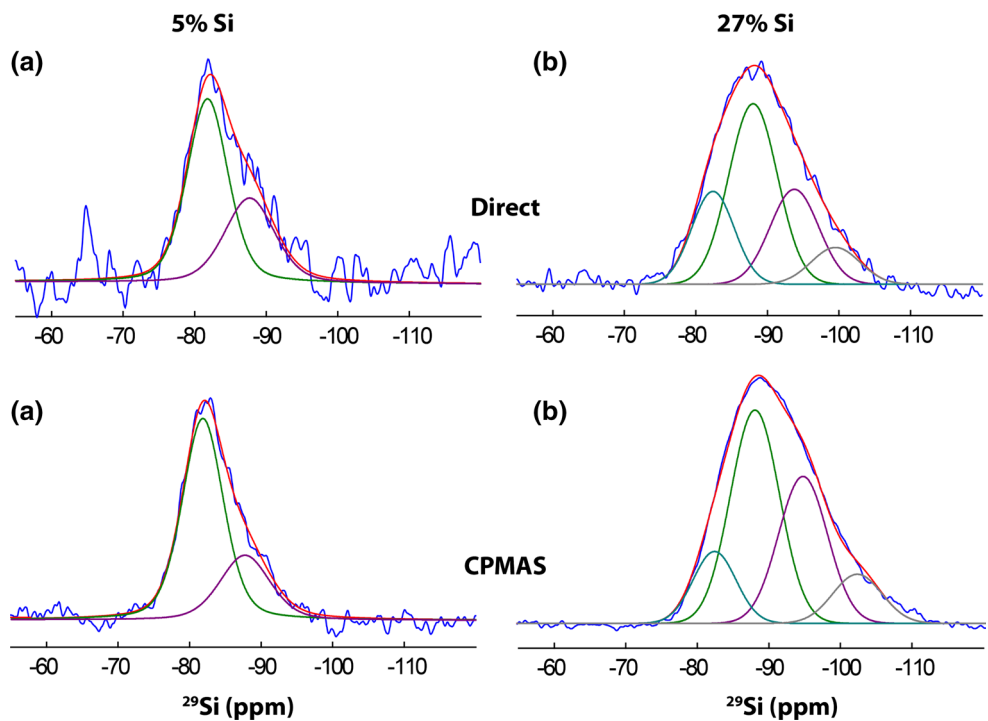
Fig. 6 The 1D ^{27}Al MAS NMR spectra for 5 and 27 % SDAs and alumina calcined at 700 and 1200 °C for 2 h



Sample ID	Calcination T °C / 2h	Al (IV)%	Al (V)%	Al (VI)%
Pure alumina	700	18	2	80
	1200	1	0	99
5% SDA	700	18	19	63
	1200	22	2	76
27% SDA	700	14	29	57
	1200	24	1	75

SDA: BYU silica doped alumina

Fig. 7 Direct ^{29}Si MAS NMR and ^{29}Si - ^1H CPMAS spectra for **a** 5 % SDA, **b** 27 % SDA calcined at 700 °C for 2 h



of a small amount of silica significantly enhances the thermal stability of the γ - Al_2O_3 lattice structure up to very high temperatures (1200 °C) without formation of α - Al_2O_3 . We suggest that Si doping may stabilize the oxygen lattice and therewith retard the γ to α phase transition (Fig. 1b). A similar conclusion has also been reported by Smith et al. [49] for the addition of lanthanum.

Thus, for the transformation of γ - to α - Al_2O_3 , more energy is needed for oxygen atoms to undergo rotations to restructure the oxygen lattice from fcc (γ - Al_2O_3) to hcp (α - Al_2O_3) and to suppress atomic diffusion of Al and O to the surface. It is known that the grain growth (α formation) and decrease in surface area are due to ionic diffusion [47]. Diffusion occurs in expanding neck regions and includes dislocations and lattice defects where alpha nucleation occurs [14]. Alpha formation or grain growth formations proceed at contacting points where defects and stresses exist [13, 17]. The NMR data in Fig. 5 confirm that pure alumina is in the hexagonal alpha phase at 1200 °C since 4-coordinated and 5-coordinated Al essentially disappear, and the distribution (line width) of the Al(IV) is significantly reduced suggesting the formation of α - Al_2O_3 , since only 6-coordinated Al exist in α - Al_2O_3 phase. However, for 5 % SDA calcined at 1200 °C, 4- and 6-coordinated Al are still present, confirming that the addition of silica to alumina stabilizes spinel γ - Al_2O_3 phase to 1200 °C, consistent with XRD and TGA-DSC results.

Evidence that the γ to α transformations are minimized in the 5 % SDA structure compared to that of pure alumina which is also shown in the TEM image (Fig. 4b) for this sample. The 5 % SDA samples have larger slab like primary particles, more stacking and fewer neck regions than pure alumina. This results in lower bulk density and less contacting points between the alumina crystallites. In this study, the preparation involving a $\text{H}_2\text{O}/\text{Al}$ ratio of 5:1 involves relatively slow hydrolysis, formation of larger plates, and 3D stacking morphology, all of which result in greater porosity [8]. This observation is consistent with the nitrogen adsorption results, since 5 % SDA has a larger pore volume than pure alumina (Table 1).

In addition to stabilizing the lattice structure of γ - Al_2O_3 , Si addition may also affect the ordering and stability of crystal agglomerates. From the NMR data (Fig. 6), the increased Al(V) concentration for 5 % $\text{SiO}_2/\text{Al}_2\text{O}_3$ treated at 700 °C relative to the undoped sample (0 % Al(V)) can be attributed to the formation of an interfacial silica–alumina phase in between primary crystallites in an agglomerate. The ^{29}Si SSNMR results also support this idea. Figure 6a show that the silica–alumina network originates in a structure consisting of Al–O–Si linkages and no separate SiO_2 phase is detected (no peak at $\delta \sim -110$ ppm) suggesting that Si incorporates into alumina structure and forming silica–alumina phase in γ - Al_2O_3 structure. Indeed,

in amorphous silica–alumina, Al(V) has been assigned to the interface between the alumina phase and a silica–alumina phase [50]. This concept is consistent with an earlier observation that addition of silica increases disordering of alumina primary particles [51]. Moreover, it is also reported that bridging Al atoms that stabilize stacking fault defects in γ - Al_2O_3 structure are Al(V) [49]. Another view is that the interfacial silica–alumina phase disrupts the γ - Al_2O_3 structure to form a new Si–Al spinel phase, consistent with data showing that alumina containing less than 28 % silica forms a Al–Si spinel structure [52]. However, commercial 5 % silica doped alumina (Siral-5) has two distinct phases (SiO_2 and Al_2O_3) [53].

The postulate of a separate silica–alumina phase at the interface of primary crystallites would suggest the possibility of different pore size regimes, which is consistent with BET data of this study showing a bimodal pore size distribution. The smaller pores in the 5 % SDA structure are in the same range as for the pure alumina and are thus characteristic of those in the basic alumina structure in both doped and pure samples. On the other hand, larger pores in 5 % SDA (i.e., 35–52 nm) can be assigned to the interfacial silica–alumina phase which apparently collapses at 1200 °C (note the absence of large pores in Table 1).

4.2 Comparison to other silica-doped alumina

Table 2 shows the specific surface area, pore volume and pore diameter of lanthanum- and silica-doped aluminas synthesized by different methods and of commercial doped aluminas calcined at 700, 1100 and 1200 °C. After treatment of 5 % SDA prepared by the method of this study at either 1100 or 1200 °C for 2 h, only the γ phase is observed; this was the case in only one previous study using cryogel methods to prepare a 10 % silica/alumina. By contrast commercial and noncommercial lanthanum- and silica-doped aluminas synthesized by other methods contain both γ and α or θ after treatment at 1100 and/or 1200 °C for 2 h. The surface and pore properties of the 5 % SDA after treatment at 1100 °C for 2 h are remarkable in comparison to the other silica-doped aluminas. The surface area of 160 m^2/g is the largest, the pore volume of 0.99 cm^3/g is 2nd largest, and the pore diameters of 22.5 and 52 nm are by far the largest. The bimodal pore size distribution is also unique.

The 5 % $\text{SiO}_2/\text{Al}_2\text{O}_3$ prepared by Horiuchi et al. [17] using supercritical drying, is uniquely stable among those prepared in previous studies. These workers reported a highly thermally stable silica-doped alumina support that remains in the θ phase after treatment at 1100 °C for 1 h with the largest pore volume of 1.3 cm^3/g compared to 0.99 cm^3/g for the 5 % SDA reported here, however the

Table 2 Surface area, pore diameter, and mesopore volume for doped aluminas with different methods at different temperatures (°C)

Sample ID	BET surface area (m ² /g)			Mesopore volume (cm ³ /g)			Pore diameter (nm)			Alumina phase	
	700	1100	1200	700	1100	1200	700	1100	1200	1100	1200
5 % Si/Al ₂ O ₃ (SDA) ^{g,a}	338	160	111	1.83	0.99	0.59	14.7 and 35.0	22.5 and 52.0	29.4	Gamma	Gamma
5 % Si/Al ₂ O ₃ (Siral-5) ^{f,a}	288	128	73	0.61	0.4	0.23	7.7	11.2	11.4	Gamma and alpha	Gamma and alpha
5 % Si/Al ₂ O ₃ [17] ^b	–	120	110	–	1.28	0.9	–	10.8	18.6	Theta	Theta
5 % Si/Al ₂ O ₃ ³⁵	–	200	150	–	–	–	–	10.8	22.8	Delta	Delta
10 % Si/Al ₂ O ₃ [20] ^c	–	100	47	–	0.2	0.1	–	3.5	3.5	Gamma	Gamma
10 % Si/Al ₂ O ₃ [15] ^a	–	–	150	–	–	0.65	–	–	–	–	Alpha and gamma
5 % Si/Al ₂ O ₃ [16] ^d	187	68	–	0.57	0.35	–	7.4	15.0	–	Alpha and theta	–
3 % La/Al ₂ O ₃ (BLDA) ^h	280	139	–	0.32	0.22	–	3.7	2.7	–	Gamma	–
3 % La/Al ₂ O ₃ [26] ^e	199	–	–	0.50	–	–	7.8	–	–	–	–
3 % La/Al ₂ O ₃ (Puralox-SCFa) ^f	174	140	–	0.50	0.5	–	11.4	16	–	–	–

Calcined for: ^a 2 h, ^b 1 h, ^c 5 h, ^d 4 h, ^e 6 h

^f Commercially available; results from this study (Puralox-SCFa: 3 % lanthanum doped alumina, and Siral5: 5 % silica doped alumina from Sasol)

^g SDA: BYU silica-doped alumina

^h BLDA: BYU lanthanum-doped alumina

pore diameter of 10 nm for their support is much smaller than the pore diameters of 5 % SDA of 22.5 and 52.0.

Table 3 shows the surface area and pore properties following very severe treatments at different temperatures for 24 h for 5 % SDA and Siral-5 (5 % silica-doped alumina from Sasol), the best commercial silica-doped support. The SDA reported here shows improvements of 46 % in surface area, 155 % in pore volume, and 94 % in pore diameter over Siral-5 after 24 h at 1100 °C. In addition, XRD data (Fig. 8a) shows that α -Al₂O₃ peaks are observed for Siral-5 calcine at 1100 °C for 24 h. In contrast, 5 %

SDA XRD shows peaks attributed to γ and traces of θ -Al₂O₃ at same temperatures (Fig. 8b). Thus the thermally stable 5 % SDA is superior to other supports in term of maintaining a high surface area and a large porosity at higher temperatures. Consequently, the increased thermal stability results in more control of the acid site properties of the SDA supports since it can be calcined at higher temperature to remove surface hydroxyl groups [54], which reduces interaction between active catalytic phase and support and therefore offers better catalytic performance in Fischer–Tropsch synthesis [55].

Table 3 BET results of 5 % SDA and Siral-5 calcine at different temperature for 24 h

Sample ID	BET surface area (m ² /g) ^a				Mesopore volume (cm ³ /g) ^a				Pore diameter (nm) ^b			
	700 °C	900 °C	1100 °C	1200 °C	700 °C	900 °C	1100 °C	1200 °C	700 °C	900 °C	1100 °C	1200 °C
5 % SDA ^c	349	270	131	61	1.06	1.11	0.84	0.24	14.7 and 35.0	19.8 and 51.8	22.5 and 51.3	15.4 and 32.2
Siral-5-Sasol ^d	262	203	90	28	0.61	0.56	0.33	0.13	8.8	10.5	12.4	18.6

^a Determined by N₂ adsorption at 77 K

^b Determined by an improved slit pore geometry (SPG) model for large pore sizes using the desorption branch

^c SDA: BYU silica doped alumina; Gamma and traces of theta alumina peaks are observed at 1100 and 1200 °C for 24 h

^d Siral-5: Commercially available 5 % silica doped alumina; alpha alumina peaks are observed at 1100 and 1200 °C for 24 h

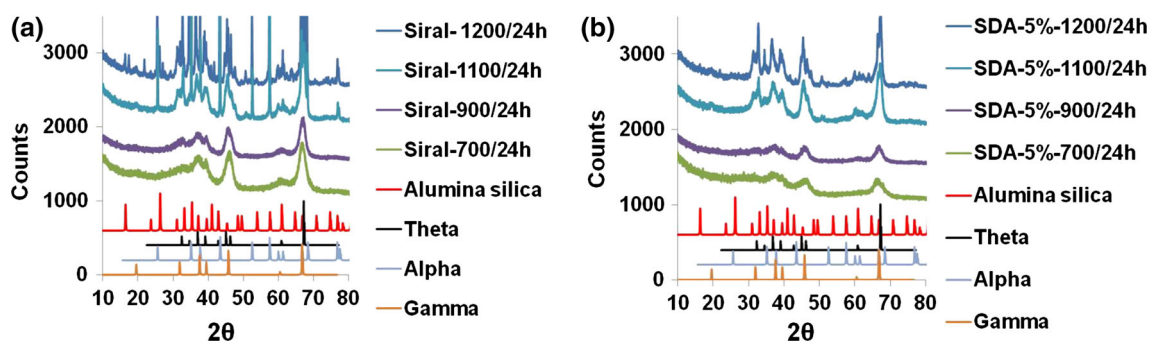


Fig. 8 XRD patterns of **a** Siral-5 calcined at different temperatures for 24 h, **b** 5 % SDA calcined at different temperatures for 24 h

5 Conclusions

In summary, we have produced a thermally stable silica-doped alumina with a high surface area, a large pore volume, and a large bimodal pore distribution via a facile, one-pot, solvent deficient method. In this study, different wt% of Si (0, 5, 15, 27) doped aluminas were synthesized and thermally treated at different temperatures (700, 800, 1100, 1200 °C). Results show that 5 wt% silica-doped alumina possesses a high surface area of 160 m²/g, large pore volume of 0.99 cm³/g, and a large bimodal pore size distribution of 23 and 52 nm after thermal treatment at 1100 °C. It remains in the gamma phase to 1200 °C.

The results of this study also provide insight into the mechanism of the stabilization of silica-doped alumina, as follows:

1. Silica stabilizes the oxygen lattice of γ -Al₂O₃ and retards the α -Al₂O₃ formation by formation of an interfacial silica–alumina phase in between primary crystallites in the agglomerate, which affects the ordering and stability of the γ -Al₂O₃ crystal agglomerates.
2. The 5 wt% silica content is enough to enter tetrahedral vacancies in the γ -Al₂O₃ structure which forms an interfacial silica–alumina phase which disrupts the γ -Al₂O₃ structure, improves stability, and forms a second large pore size distribution in the structure.

In terms of applications, silica-doped aluminas prepared via this facile, one-pot method, have favorable pore properties and excellent thermal stability. Therefore, it is the ideal catalyst support for high temperature applications, including automobile emission control, hydrotreating of petroleum feedstocks (hydrodesulphurization), and Fischer–Tropsch synthesis.

Acknowledgments This work was supported by the U.S. Department of Energy under grant DE-FG02-05ER15666 and National Science Foundation under CHE-0959862. The solid state NMR (TMA) was performed at Sandia National Laboratories which is a

multi-program laboratory managed and operated by Sandia Corporation, a wholly owned subsidiary of Lockheed Martin Corporation, for the U.S. Department of Energy’s National Nuclear Security Administration under contract DE-AC04-94AL85000. We also thank Dr. Jeff Farrer and the BYU microscopy lab for their assistance with the TEM imaging.

References

1. M. Ozawa, Thermal stabilization of catalytic compositions for automobile exhaust treatment through rare earth modification of alumina nanoparticle support. *J. Alloys Compd.* **408–412**, 1090–1095 (2006)
2. H. Pines, W.O. Haag, Alumina: catalyst and support. IX. The alumina catalyzed dehydration of alcohols. *J. Am. Chem. Soc.* **83**, 2847–2852 (1961)
3. O.V. Klimov, M.A. Fedotov, A.V. Pashigreva, S.V. Budukva, E.N. Kirichenko, G.A. Bukhtiyarova, A.S. Noskov, Complexes forming from ammonium paramolybdate, orthophosphoric acid, cobalt or nickel nitrate, and carbamide in solution and their use in the preparation of diesel fuel hydrodesulfurization catalysts. *Kinet. Catal.* **50**, 867–873 (2009)
4. C.H. Bartholomew, R.J. Farrauto, *Fundamentals of Industrial Catalytic Processes*, 2nd edn. (John Wiley & Sons Inc., Hoboken, NJ, 2006)
5. A.R. de la Osa, A. de Lucas, A. Romero, J.L. Valverde, P. Sanchez, Influence of the catalytic support on the industrial Fischer–Tropsch synthetic diesel production. *Catal. Today* **176**, 298–302 (2011)
6. B.F. Woodfield, S. Liu, J. Boerio-Goates, Q. Liu, *Preparation of Uniform Nanoparticles of Ultra-High Purity Metal Oxides, Mixed Metal Oxides, Metals, and Metal Alloys II*, 2006
7. B.F. Woodfield, C.H. Bartholomew, B. Huang, R.E. Olsen, L. Astle, *Method for making highly porous, stable metal oxide with a controlled pore structure*, vol. 40, (WO Application Brigham Young University, 2011)
8. B. Huang, C.H. Bartholomew, S.J. Smith, B.F. Woodfield, Facile solvent-deficient synthesis of mesoporous gamma alumina with controlled pore structures. *Microporous Mesoporous Mater.* **165**, 70–78 (2013)
9. J. Cejka, Organized mesoporous alumina: synthesis, structure and potential in catalysis. *Appl. Catal. A* **254**, 327–338 (2003)
10. C. Morterra, G. Magnacca, A case study: surface chemistry and surface structure of catalytic aluminas, as studied by vibrational spectroscopy of adsorbed species. *Catal. Today* **27**, 497–532 (1996)
11. R.K. Oberlander, Aluminas for catalysts: their preparation and properties. *Appl. Ind. Catal.* **3**, 63–112 (1984)

12. J.W. Curley, M.J. Dreelan, O.E. Finlayson, High temperature stability of alumina fiber. *Catal. Today* **10**, 401–404 (1991)
13. T. Fukui, M. Hori, Thermal stability of aluminas by hydrothermal treatment of an alkoxide-derived gel. *J. Mater. Sci.* **30**, 1794–1800 (1995)
14. T. Horiuchi, T. Osaki, T. Sugiyama, H. Masuda, M. Horio, K. Suzuki, T. Mori, T. Sago, High surface area alumina aerogel at elevated temperatures. *J. Chem. Soc. Faraday Trans.* **90**, 2573–2578 (1994)
15. J.B. Miller, E.I. Ko, A homogeneously dispersed silica dopant for control of the textural and structural evolution of an alumina aerogel. *Catal. Today* **43**, 51–67 (1998)
16. A.A. Shutilov, G.A. Zenkovets, S.V. Tsybulya, V.Y. Gavrilov, Effect of silica on the stability of the nanostructure and texture of fine-particle alumina. *Kinet. Catal.* **53**, 125–136 (2012)
17. T. Horiuchi, L. Chen, T. Osaki, T. Sugiyama, K. Suzuki, T. Mori, A novel alumina catalyst support with high thermal stability derived from silica-modified alumina aerogel. *Catal. Lett.* **58**, 89–92 (1999)
18. A.W. Espie, J.C. Vickerman, Aluminas modified with silica. Part I. An X-ray diffraction and secondary-ion mass spectrometry study of the influence of preparation and thermal treatment on structure and surface composition. *J. Chem. Soc. Faraday Trans.* **80**, 1903–1913 (1984)
19. J. Klein, W.F. Maier, Thermal stability of sol–gel-derived porous AM- Al_xZr mixed oxides. *Chem. Mater.* **11**, 2584–2593 (1999)
20. T. Osaki, K. Nagashima, K. Watari, K. Tajiri, Silica-doped alumina cryogels with high thermal stability. *J. Non-Cryst. Solids* **353**, 2436–2442 (2007)
21. J.-H. Lee, S.-C. Choi, D.-S. Bae, K.-S. Han, Synthesis and microstructure of silica-doped alumina composite membrane by sol–gel process. *J. Mater. Sci. Lett.* **18**, 1367–1369 (1999)
22. G. Lopez-Granada, J.D.O. Barceinas-Sanchez, R. Lopez, R. Gomez, High temperature stability of anatase in titania-alumina semiconductors with enhanced photodegradation of 2,4-dichlorophenoxyacetic acid. *J. Hazard. Mater.* **263**, 84–92 (2013)
23. X. Jiang, B.P. Bastakoti, W. Weng, T. Higuchi, H. Oveisi, N. Suzuki, W.-J. Chen, Y.-T. Huang, Y. Yamauchi, Preparation of ordered mesoporous alumina-doped titania films with high thermal stability and their application to high-speed passive-matrix electrochromic displays. *Chem. Eur. J.* **19**, 10958–10964 (2013)
24. T. Horiuchi, Y. Teshima, T. Osaki, T. Sugiyama, K. Suzuki, T. Mori, Improvement of thermal stability of alumina by addition of zirconia. *Catal. Lett.* **62**, 107–111 (1999)
25. R.H.R. Castro, S.V. Ushakov, L. Gengembre, D. Gouvea, A. Navrotsky, Surface energy and thermodynamic stability of gamma-alumina: effect of dopants and water. *Chem. Mater.* **18**, 1867–1872 (2006)
26. Z. Cai, J. Li, K. Liew, J. Hu, Effect of La_2O_3 -doping on the Al_2O_3 supported cobalt catalyst for Fischer–Tropsch synthesis. *J. Mol. Catal. A Chem.* **330**, 10–17 (2010)
27. C.L. Carnes, P.N. Kapoor, K.J. Klabunde, J. Bonevich, Synthesis, characterization, and adsorption studies of nanocrystalline aluminum oxide and a bimetallic nanocrystalline aluminum oxide/magnesium oxide. *Chem. Mater.* **14**, 2922–2929 (2002)
28. M. Schoeneborn, A. Paeger, R. Gloeckler, *Ceria zirconia alumina composition with enhanced thermal stability* (Sasol Germany GmbH, Germany). Application: DE, 2013
29. K. Scherzmanz, A. Sagar, M. Schoeneborn, R. Gloeckler, K. Dallmann, F. Alber, S. Rolfs, *Ceria zirconia alumina composition with enhanced thermal stability* (Treibacher Industrie AG, Austria; Sasol Germany GmbH). Application: WO, 2013
30. R.J. Nozemack, J.F. Porinchak, *Alumina-silica cogel* (W. R. Grace&Co, Newyork, NY, 1988)
31. H.K.C. Timken, *Homogeneous Modified-Alumina Fischer–Tropsch Catalyst Supports* (Chevron U.S.A. Inc., USA). Application: US, 2005
32. C.Z. Wan, J.C. Dettling, *Stabilized Alumina Catalyst Support Coatings* (Engelhard Corp., USA). Application: EP, 1986
33. T. Fukui, M. Hori, Control of micropore size distribution in alumina by the hydrothermal treatment of an alkoxide derived-alcogel. *J. Mater. Sci.* **31**, 3245–3248 (1996)
34. X. Zhao, Y. Cong, Y. Huang, S. Liu, X. Wang, T. Zhang, Rhodium supported on silica-stabilized alumina for catalytic decomposition of N_2O . *Catal. Lett.* **141**, 128–135 (2011)
35. T. Horiuchi, T. Osaki, T. Sugiyama, K. Suzuki, T. Mori, Maintenance of large surface area of alumina heated at elevated temperatures above 1300 °C by preparing silica-containing pseudoboehmite aerogel. *J. Non-Cryst. Solids* **291**, 187–198 (2001)
36. M.K. Mardkhe, B.F. Woodfield, C.H. Bartholomew, *A method of producing thermally stable and high surface area Al_2O_3 catalyst supports* (Brigham Young University, 2013)
37. B. Huang, C.H. Bartholomew, B.F. Woodfield, Facile synthesis of mesoporous γ -alumina with tunable pore size: the effects of water to aluminum molar ratio in hydrolysis of aluminum alkoxides. *Microporous Mesoporous Mater.* **183**, 37–47 (2014)
38. A.L. Patterson, The Scherrer formula for X-ray particle size determination. *Phys. Rev.* **56**, 978–982 (1939)
39. B. Huang, C.H. Bartholomew, B.F. Woodfield, Improved calculations of pore size distribution for relatively large, irregular slit-shaped mesopore structure. *Microporous mesoporous Mater.* **184**, 112–121 (2014)
40. B. Bureau, G. Silly, J.Y. Buzaré, C. Legein, D. Massiot, From crystalline to glassy gallium fluoride materials: an NMR study of ^{69}Ga and ^{71}Ga quadrupolar nuclei. *Solid State NMR* **14**, 191–202 (1999)
41. D. Massiot, F. Fayon, M. Capron, I. King, S. Le Calvé, B. Alonso, J.O. Durand, B. Bujoli, Z. Gan, G. Hoatson, Modelling one and two-dimensional solid-state NMR spectra. *Magn. Reson. Chem.* **40**, 70–76 (2002)
42. D.R. Neuville, L. Cormier, D. Massiot, Al environment in tectosilicate and peraluminous glasses: A ^{27}Al MQ-MAS NMR, Raman, and XANES investigation. *Geochim. Cosmochim. Acta* **68**, 5071–5079 (2004)
43. H. Yong, D. Coster, F.R. Chen, J.G. Davis, J.J. Fripiat, Aluminum coordination and Lewis acidity in aluminas and steamed zeolites. *Stud. Surf. Sci. Catal.* **75**, 1159–1170 (1993)
44. W.E.E. Stone, G.M.S. El Shafei, J. Sanz, S.A. Selim, Association of soluble aluminum ionic species with a silica-gel surface: a solid-state NMR study. *J. Phys. Chem.* **97**, 10127–10132 (1993)
45. L.M. Bronstein, D.M. Chernyshov, R. Karlinsey, J.W. Zwanziger, V.G. Matveeva, E.M. Sulman, G.N. Demidenko, H.-P. Hentze, M. Antonietti, Mesoporous alumina and aluminosilica with Pd and Pt nanoparticles: structure and catalytic properties. *Chem. Mater.* **15**, 2623–2631 (2003)
46. R.X. Fischer, H. Schneider, M. Schmucker, Crystal structure of Al-rich mullite. *Am. Mineral.* **79**, 983–990 (1994)
47. P. Burtin, J.P. Brunelle, M. Pijolat, M. Soustelle, Influence of surface area and additives on the thermal stability of transition alumina catalyst supports. II. Kinetic model and interpretation. *Appl. Catal.* **34**, 239–254 (1987)
48. T. Mori, T. Horiuchi, T. Iga, Y. Murase, Large surface area of silica-coated fibrous crystals of alumina after heating at >1573 K. *J. Mater. Chem.* **2**, 577–578 (1992)
49. J.S. Smith, *The synthesis and structural characterization of metal oxide nanoparticles having catalytic applications* (Brigham Young University, 2012)

50. E.J.M. Hensen, D.G. Poduval, P.C.M.M. Magusin, A.E. Coumans, J.A.R. van Veen, Formation of acid sites in amorphous silica–alumina. *J. Catal.* **269**, 201–218 (2010)
51. L.L.L. Prado, P.A.P. Nascente, S.C. De Castro, Y. Gushikem, Aluminium oxide grafted on silica gel surface: study of the thermal stability, structure and surface acidity. *J. Mater. Sci.* **35**, 449–453 (2000)
52. A.K. Chakraborty, Range of solid solutions of silica in spinel type phase. *Adv. Appl. Ceram.* **105**, 297–303 (2006)
53. W. Daniell, U. Schubert, R. Glockler, A. Meyer, K. Noweck, H. Knozinger, Enhanced surface acidity in mixed alumina-silicas: a low-temperature FTIR study. *Appl. Catal. A* **196**, 247–260 (2000)
54. M.K. Mardkhe, K. Keyvanloo, C.H. Bartholomew, W.C. Hecker, T.M. Alam, B.F. Woodfield, Acid site properties of thermally stable, silica-doped alumina as a function of silica/alumina ratio and calcination temperature. *Appl. Catal. A* **482**, 16–23 (2014)
55. K. Keyvanloo, M.K. Mardkhe, T.M. Alam, C.H. Bartholomew, B.F. Woodfield, W.C. Hecker, Supported iron Fischer–Tropsch catalyst: superior activity and stability using a thermally stable silica-doped alumina support. *ACS. Catal.* **4**, 1071–1077 (2014)